Journal of Theoretical Biology 534 (2022) 110946

Contents lists available at ScienceDirect

Journal of Theoretical Biology

journal homepage: www.elsevier.com/locate/yjtbi

Non-cooperative mechanism for bounded and ultrasensitive chromatin remodeling

Alvaro Fletcher [a], Ruonan Zhao [b], German Enciso [b,*]

[a] Mathematical, Computational, and Systems Biology program, University of California, Irvine, Irvine, CA, USA
[b] Department of Mathematics, University of California, Irvine, Irvine, CA, USA

ARTICLE INFO

Article history:
Received 21 May 2021
Revised 19 October 2021
Accepted 22 October 2021
Available online 28 October 2021

Keywords:
Chromatin remodeling
Ultrasensitivity
Percolation
Cooperativity

ABSTRACT

Chromatin remodeling is an essential form of gene regulation that is involved in a variety of biological processes. We develop a theoretical model that takes advantage of percolation effects at the level of nucleosome interactions, which allows for ultrasensitive chromatin expansion. This model is non-cooperative and readily provides spatial bounds to the expansion region, preventing uncontrolled remodeling events. We explore different chromatin architectures and the ultrasensitivity of the chromatin density as a function of transcription factor concentration. We also compare our model with experimental data involving an inhibitor of nucleosome acetylation. These results suggest a novel mechanism for spatially-bounded chromatin remodeling and they provide means for quantitative comparisons between proposed models of chromatin architecture.

1. Introduction

Chromatin remodeling is used by many organisms as an important form of gene regulation, expanding or compacting DNA to tallow or prevent access to genetic regions. Chromatin changes between high and low density states respectively known as heterochromatin and euchromatin, with high density heterochromatin typically silencing gene expression. The boundaries between these regions have been observed to be sharp, and their disruption has been associated with conditions such as growth defects (Honda et al., 2010; Wei et al., 2005).

Much experimental progress has been made in understanding the regulation of sharp boundaries between euchromatin and heterochromatin (Li and Zhou, 2013; Tamaru, 2010; Wang et al., 2012; Wang et al., 2014). On the modeling side, previous work on transitions between chromatin states has mostly relied on cooperative assumptions to obtain ultrasensitive transitions (Michieletto et al., 2016; Mirny, 2010; Schwämmle and Jensen, 2013; Sneppen et al., 2008).

Erdel and Greene (2016) showed that a non-cooperative looping model was able to create an extended domain of modified nucleosomes. This model makes use of the contact probabilities between two chromatin segments to determine the rates of histone modification. However among models of ultrasensitive behavior, cooperativity or allostery is usually assumed. For instance, work by Sneppen et al. (2008) modeled cooperative histone modifications, and it is ultrasensitive but potentially subject to uncontrolled chromatin expansion beyond the intended boundaries of gene expression. In order to correct for this, more recent work (Dodd and Sneppen, 2011) accounts for spatially bounded chromatin remodeling through the introduction of silencer elements and barriers. Modeling work by Mirny (2010) includes allosteric binding of transcription factors which sterically hinders DNA interactions. Additional work includes models of bounded chromatin modification, such as (Erdel and Greene, 2016; Hodges and Crabtree, 2012; Mukhopadhyay and Sengupta, 2013) in which nearest neighbor interactions are used in a cooperative manner, and the work by Jost and Valliant (Jost and Vaillant, 2018) in which long range interactions are considered for chromatin expansion. For instance, Hodges and Crabtree (2012) focus on the bounded nature of modifications with nucleation, nearest neighbor cooperativity, and first-order turnover.

In this work, we present an alternative non-cooperative model that produces sharp spatial bounds and ultrasensitive transitions in response to transcription factors. This approach has the added advantage of not requiring silencer elements or barriers to prevent uncontrolled chromatin expansion. We will operate under the hypothesis that histone modifications are independent from one another. In other words, our model assumes that the modification of any one histone does not influence the rate of modification for any other histone. Our model has the potential to complement

* Corresponding author.
E-mail address: enciso@uci.edu (G. Enciso).

https://doi.org/10.1016/j.jtbi.2021.110946
0022-5193/

cooperative models, and it can be particularly helpful in circumstances where experimental data indicate a lack of cooperativity.

Unlike Erdel and Greene (2016), our non-cooperative approach relies on the acetylation range of HAT proteins (Vignali et al., 2000) and emergent properties of the chromatin architecture. The chromatin boundaries remain sharp even without the involvement of barrier proteins, and no uncontrolled expansion is possible beyond the regulated regions. Moreover, a single HAT protein bound at a DNA site can make accessible hundreds of DNA base pairs, a longer range of interaction than steric transcription factor binding. Two mechanisms allow for this in our model, namely percolation effects and multisite histone tail modifications.

To develop an intuition for the concept of percolation, consider a body of water being pushed under pressure through porous soil. The water will flow from the top to the bottom of the soil only if there are sufficiently many connected pores to form a path. As the prevalence of pores inside the soil increases, it is well known that the probability for a path increases in an ultrasensitive manner (Saberi, 2015). That is, a small increase in the pore prevalence can lead to a large increase in the probability of water flow.

The chromatin, despite having a high number of close range interactions, has yet to be studied in the context of percolation to the best of our knowledge. Unlike the soil, the presence of linker DNA between the nucleosomes implies that there is always a path between the two ends of the DNA. To address this issue, we turn to measuring the length of the shortest such path under different levels of acetylation. We show that the ultrasensitivity derived from the percolation analysis is conserved by using this measurement. Hence, in a similar way to the percolation in the soil, the first few nucleosome acetylation events in a high density region of chromatin will have a limited effect. But once the acetylation events reach a critical number, they can suddenly lead to a large expansion of the chromatin.

Levels of ultrasensitivity were further increased by multisite effects at the level of histone tail modification. Each nucleosome has eight different histones and at least eight histone tails, some of which in turn may have multiple acetylation sites. While each acetylation may increase the tendency for nucleosomes to detach from the chromatin, we assume that a sufficient number of acetylation events must take place between two nucleosomes before their interaction is affected. This mechanism is based on work of Wang et al. (2010) in the context of multisite protein phosphorylation but applies equally well in this different system. Ultrasensitivity is increased once again without the need to assume cooperative interactions between the histone tails, although such interactions could further increase ultrasensitive responses.

We also include a comparison with an experimental system involving histone acetylation inhibitor drug mitoxantrone. By including additional reactions in our mathematical model to account for the presence of this inhibitor, we were able to closely reproduce the experimental dose response relation. A high Hill coefficient of 3.8 indicates that this system is ultrasensitive, and we postulate that this behavior may be due to the effects described above.

We begin with Section 2 by providing background on chromatin architectures and the role of histone acetylation in chromatin remodeling. In Section 3.1, we describe in more detail on how we represented chromatin as a graph. In particular, we define the shortest path from one end of DNA to the other as a proxy to measure chromatin density. Section 3.2 introduces the idea of percolation and its relationship to the model. In Section 3.3 we outline the multisite assumptions for nucleosome interactions and demonstrate the ultrasensitive relation between the probability of acetylation and DNA accessibility. In Section 4.1 we display the activity domain of a HAT protein (Vignali et al., 2000) and the results of incorporating such data into the model. Section 4.2 constructs a reaction network in order to derive the probability of histone acetylation from a transcription factor input. Section 4.3 calculates an ultrasensitive response in chromatin accessibility as a function of transcription factor concentration. In Section 4.4 we examine the ultrasensitivity of the transcription factor dose response for different model parameters. Lastly, in Section 4.5 we reproduce data measured experimentally for a similar system involving inhibitor drug mitoxantrone.

2. Biological background

The eukaryotic nucleus accommodates large amounts of DNA by packaging it into a form known as chromatin, which can have different levels of density. DNA is usually wrapped around histone octamers forming structures known as nucleosomes. When DNA is tightly packed around the nucleosomes it forms a dense version of the chromatin known as heterochromatin or 30 nm chromatin fiber, named after its diameter when observed under an electron microscope (Felsenfeld and McGhee, 1986). For a region of DNA to be actively expressed, the corresponding chromatin region usually needs to be loosened into a lower density state known as euchromatin or 10 nm chromatin fiber. While the shape of the 10 nm fiber is well-characterized to the point that it has been described as “beads-on-a-string” (Marion and Roux, 1980), it still remains unclear what shape the chromatin takes as a 30 nm fiber when it is compact and the corresponding DNA regions are silenced (Zhou et al., 2018).

The existence of the 30 nm chromatin structure has been disputed (Fussner et al., 2012; Maeshima et al., 2019; Maeshima et al., 2014; Ricci et al., 2015; Maeshima et al., 2010; Ou et al., 2017), and it has been theorized that 30 nm fibers could consist of an irregular pattern of interdigitated 10 nm fibers (Quénet et al., 2012). Recent research studying gene regulation has uncovered an important role for so-called *enhancers*, which are segments of DNA that regulate genes located outside of the promoter DNA region. In many cases these enhancer regions regulate their targets by being physically located near the promoter in their 3D structure. This indicates that the 3D chromatin structure might be highly regulated and conserved. The presented work can easily be extended to such a situation, by defining a 3D chromatin structure interaction graph. Several other models for the shape of the 30 nm fiber have been proposed, among them the solenoid model and the zig-zag model which themselves can be modified to form different kinds of models (Finch and Klug, 1976; Wu and Bassett, 2007).

It has been hypothesized that heterochromatin is able to remain compact due to interactions between neighboring nucleosomes (Pepenella et al., 2014). In particular, it is thought that the histone tails, which extend from the nucleosome center, are able to interact with other histone tails, enabling communication between nucleosomes that are far apart relative to their position in the DNA (Krajewski, 2016; Kulaeva et al., 2012). Therefore, nucleosomes are partially reliant on the state of their neighbors for maintaining a particular state of chromatin compaction under certain conditions.

One condition that determines the presence of nucleosome interactions is the acetylation of the histone tails. Acetylation can weaken the attraction between the positively charged histones and the negatively charged DNA, thereby breaking nucleosome bonds, loosening the chromatin, and facilitating the transition from heterochromatin to euchromatin (Bannister and Kouzarides, 2011; Kan et al., 2009; Lee et al., 2011; Li and Kono, 2016; Szerlong et al., 2010). Once euchromatin is present, the regulatory elements of transcription can more easily bind to the DNA and start the

production of mRNA (Görisch et al., 2005). This way, high levels of acetylation around a gene locus are thought to facilitate transcription.

Transcription is regulated to take place at specific regions in order to prevent uncontrolled global expression of the DNA. This is possible because of transcription factors which selectively bind to chromatin regions that need to be decompressed (Fry and Peterson, 2001; Legube and Trouche, 2003). These transcription factors, once bound to the DNA, recruit histone acetyltransferases (HATs) which then proceed to acetylate histone tails (Marmorstein and Roth, 2001). This way, only regions that have a specific transcription factor binding site will be capable of being decompressed and subsequently expressed (Fig. 1).

3. Chromatin model

3.1. Chromatin as a graph

For a mathematical description of the chromatin, we create a 2D graph of nucleosomes connected by linker DNA and capable of nucleosome interactions, which aims to capture the 3D structure of different chromatin architectures. The nucleosomes are depicted as red nodes while the linker DNA and the nucleosome interactions are shown as black and green edges in Figs. 2b and 2d. Importantly, acetylation events tend to *reduce* the presence of green edges.

We use two alternative chromatin structures for our analysis, the so-called *interdigitation* (Fig. 2)a and *solenoid* (Fig. 2c) models. We choose the solenoid model since it is perhaps the best-known chromatin model. Moreover, we also use an interdigitation model because of its simplicity and because it is not a traditional 30 nm model. The latter point is important since the existence of 30 nm fibers *in situ* has been disputed (Fussner et al., 2012; Maeshima et al., 2014; Maeshima et al., 2019; Ricci et al., 2015; Maeshima et al., 2010; Ou et al., 2017) and the interdigitation model as an arrangement of 10 nm fibers has been proposed as one of the alternatives to the 30 nm fibers. We note, however, that our approach can be generalized to any chromatin model by simply changing the structure of our graph to describe the interactions among histones, even in a non-uniform fashion.

The nucleosomes in both models have distinct conformations, and each nucleosome has a different set of neighbors. The interdigitation model describes a chromatin where nucleosomes are arranged in a shape similar to the fingers of two hands being interlocked. In the solenoid model, nucleosomes are arranged in a 3D spiral shape. Each of these topologies determines which nucleosome interactions are possible and consequently affects the rate of transitions between chromatin density states.

Given a graph with a particular set of nucleosome interactions, an important problem is to quantitatively measure the overall chromatin density, which inversely correlates with gene activation levels. We estimate chromatin density by calculating the length of the *shortest path* from one end of the DNA sequence to the other, also known as the diameter of the graph. For example, consider an interdigitation graph with nodes arranged in n rows and m columns. If n is even, the length of the shortest path would be $n-1$ under no acetylation (all green edges present). Meanwhile if n is odd, the length of the shortest path when all edges are present is $n-1+m-1$. On the other hand, under complete acetylation (no green edges present), the shortest path is the length of the entire DNA sequence, that is $nm-1$, regardless of the parity of n. Note that highly acetylated chromatin (euchromatin) will correspond to larger diameters since nucleosome interactions will be less abundant. On the other hand, non-acetylated chromatin (heterochromatin) will correspond to smaller diameters since nucleosome interactions will be more abundant.

3.2. Percolation theory

Consider water flowing through the soil to an unconfined aquifer (Fig. 3a). The water flows through passages until it reaches the aquifer. To capture this behavior, we can represent the soil as a two-dimensional graph where the edges between nodes correspond to water passages between two different locations (Fig. 3b). From such a graph, one can determine if a path exists from the top row to the bottom row and determine the shortest path between these two rows.

We generalize the graph in Fig. 3b by considering a grid with 9 rows and 5 columns. Suppose that each edge between two neighboring nodes (vertical or horizontal) is present with a given probability, independently of each other. Probabilities with high values can be expected to lead to more edges and highly interconnected graphs while low probabilities can be expected to create few edges and poorly connected graphs. Such an experiment can be repeated for distinct probabilities and, for each unique probability, the existence of a path from the top row to the bottom row is recorded (Fig. 3c).

In the percolation problem of the soil, a path may or may not exist, depending on the distribution of pores within the soil. However, our chromatin architecture always has a path from the top row to the bottom row, which is guaranteed by the presence of linker DNA. As a consequence, the model of the soil differs from our chromatin architecture. Thus, we want to use a new metric to describe our problem of chromatin expansion. In order to resolve this problem, we turn our attention to the diameter of the graph as defined in the previous section. We show below that if the

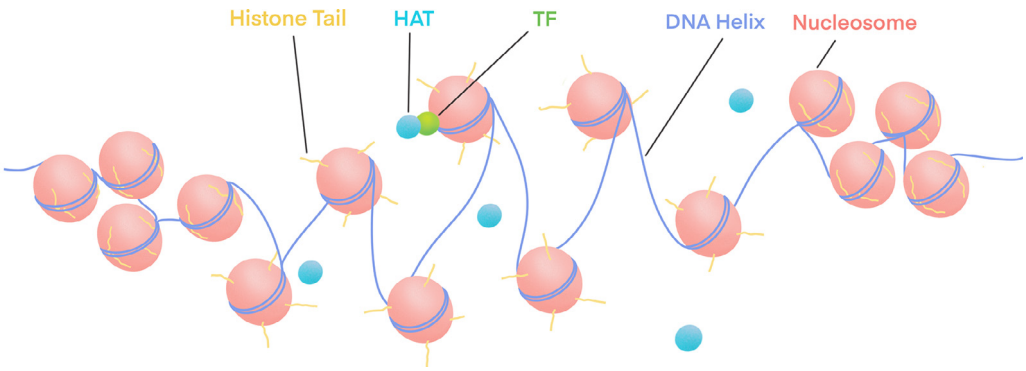

Fig. 1. HAT proteins are recruited by site-specific transcription factors (TFs). Once bound to the chromatin, HAT proteins acetylate nearby histone tails, which can lead to chromatin decompression.

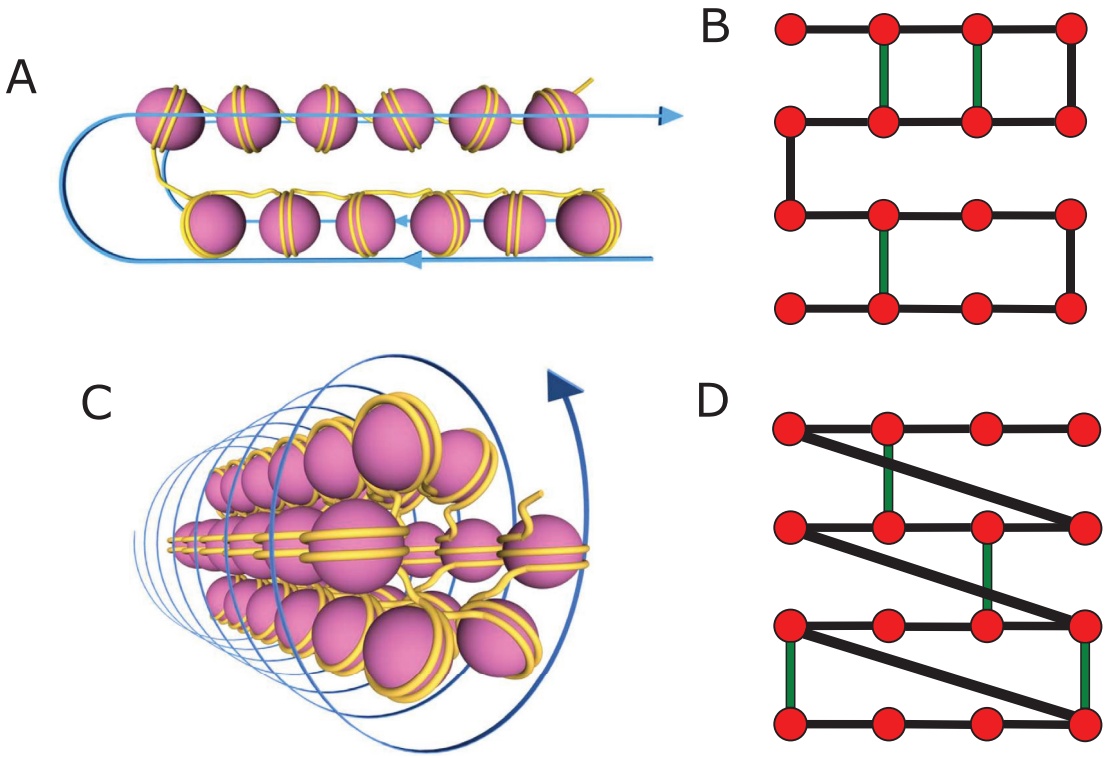

Fig. 2. (A) The interdigitation architecture has been proposed to describe the 30 nm chromatin structure. Nucleosomes can interact with their neighbors depending on their level of acetylation. (B) Interdigitated DNA represented using an abstract graph. Red nodes correspond to nucleosomes, black edges to linker DNA, and green edges to nucleosome interactions. The shortest path between the two ends of the DNA (DNA diameter) provides a convenient way to estimate chromatin density. (C) Solenoid chromatin architecture. (D) Representation of the solenoid architecture using a similar graph and notation as in (B).

probability of path existence is replaced with a measurement of the mean graph diameter, then the same ultrasensitive response is preserved.

For the same random graph as above, the mean shortest path length is calculated after several simulations for a fixed edge probability. We use a procedure known as *Dijkstra's algorithm* to quickly compute the shortest path (Cormen, YYYY). If no path existed, then we record the length of the longest possible path (36 in this case).

This is akin to the chromatin graphs in Fig. 2 where having no edges implies the longest path is the diameter of the graph. After normalizing path lengths to 1, they are plotted alongside the probability of path existence as in Fig. 3c.

Notice that both of the graphs in Fig. 3c observe an ultrasensitive behavior. It has been proved in the literature that as the size of a square grid grows, the probability of path existence becomes increasingly and arbitrarily ultrasensitive (Saberi, 2015).

In Fig. 3d we plot the mean shortest path length and the probability of path existence in the same graph. Notice that there appears to be a linear relationship between the two. Indeed, suppose M, Q are the mean shortest path length and the probability of path existence, respectively. The formula $M = 1 - aQ$ would imply that if one of these two functions is ultrasensitive as a function of edge probability, then so is the other.

3.3. Formation of nucleosome interactions

Nucleosomes can form interactions between them, shown as green edges in Figs. 2b and 2d. We assume that nucleosomes placed diagonally from each other cannot interact, and nucleosomes placed horizontally from each other are already connected by linker DNA (black edges). Therefore, only vertical neighbors are allowed to form nucleosome interactions.

In the text below we define the concept of nucleosome receptiveness, which broadly speaking means that a nucleosome has a limited number of acetylated sites. Any two neighboring nucleosomes are then joined by a green edge if and only if both of the nucleosomes are receptive.

We assume that there are s acetylation sites in each nucleosome, and we define the nucleosome to be *receptive* if at least k out of these s sites were non-acetylated. We set $s = 8$ since there are eight histones in every nucleosome, and we thought of each histone as having one acetylation site in its tail. In reality, the number of acetylation sites in a nucleosome could be higher as multiple sites have been identified in the H4, H3, H2A, and H2B histones (Barnes et al., 2019; Kurdistani et al., 2004). To account for this variability, the model can be given any positive number of sites s depending on the system being modeled.

Define p to be the probability of acetylation of a given histone site. Unlike in cooperative models, we assume here that histone acetylations are independent from each other. Therefore, the number W of non-acetylated histone sites in a nucleosome has a binomial distribution, and the probability of a nucleosome being receptive can be calculated as

$$\begin{aligned} P(W \geqslant k) &= P(W = k) + P(W = k+1) + \ldots + P(W = s) \\ &= \sum_{i=k}^{s} \binom{s}{i} q^i p^{s-i}, \end{aligned} \tag{1}$$

where $q = 1 - p$. We also set $k = 4$, which is consistent with previous work on multisite modification systems where the probability of transition to another state is given by Eq. (1) (Wang et al., 2010). This work showed that the ultrasensitivity of the resulting dose response was maximized for $k \approx s/2$. Hence, only when sufficient histone sites are not acetylated as given by equation (1) does a nucleosome become receptive and is able to form green edges with

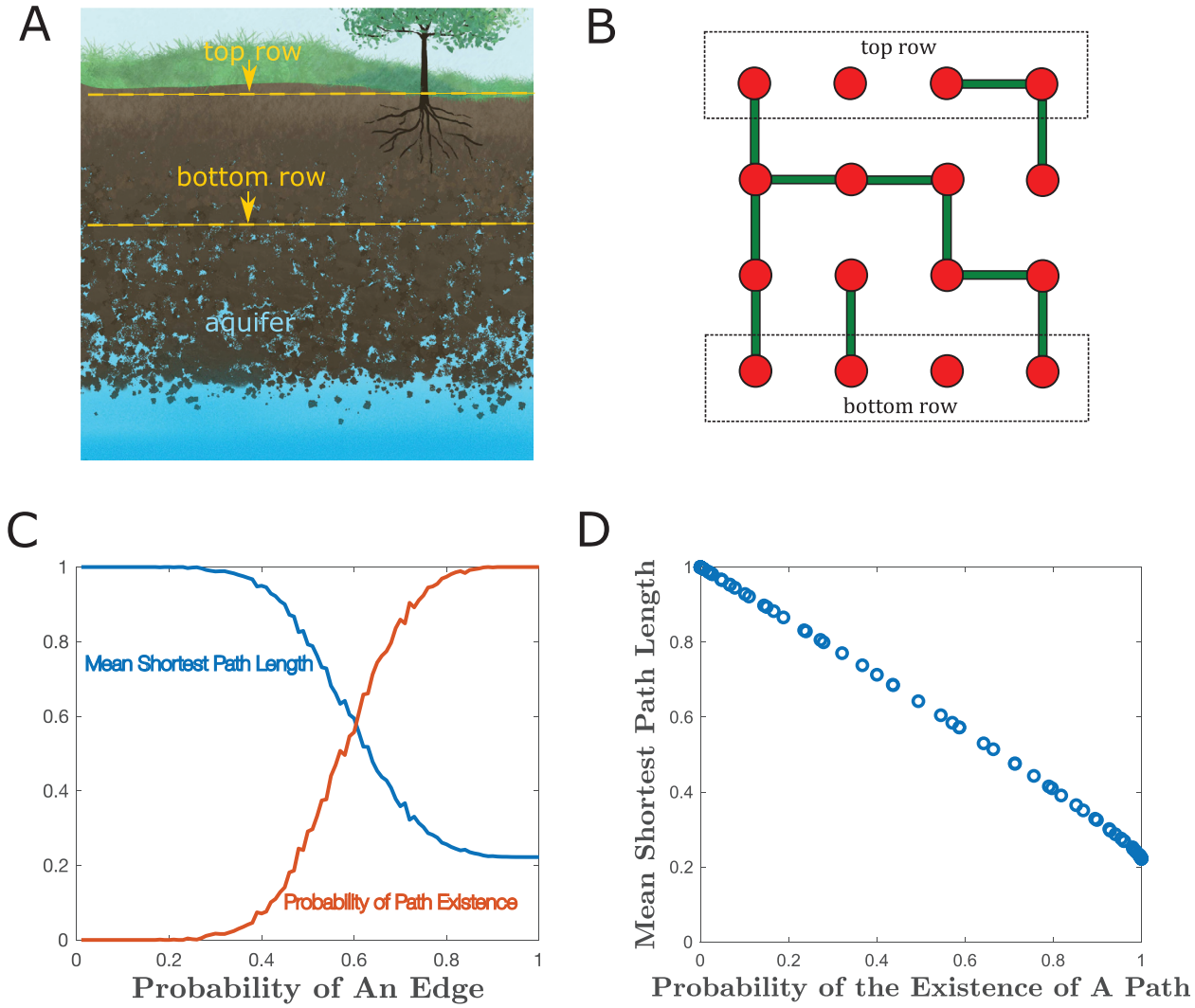

Fig. 3. (A) Water flows from the soil surface to an aquifer through passages in the soil. (B) A graph representation of the soil where water passages are shown as edges between nodes. In this case there exist two paths from the surface (top row) to the aquifer (bottom row), and the shortest path has length 3. (C) Normalized mean shortest path lengths and probabilities of path existence for a 9×5 graph. Each data point is calculated using 1000 independent simulations for each edge probability. (D) The relationship between mean shortest path lengths and the probability of path existence.

its receptive neighbors. Note that the number of acetylation sites is the same for all nucleosomes, and it is therefore independent of the number of neighboring nucleosomes.

There is experimental evidence in support of this set of assumptions. Durrin et al. (1991) and Schreiber and Bernstein (2002) considered different acetylation sites in the tail of histone H4, and when any one of these sites was shut down (by replacement of the lysine residue with arginine which mimics the nonacetylated state), no significant effect was measured in gene expression. However when three or four sites were eliminated in this way, gene expression was significantly decreased. This experiment effectively estimated the number $k = 4$ of nonacetylated sites that are necessary and sufficient to make a histone receptive in our context. If $s = 8$ and $k = 4$, then replacing e.g. two lysine residues with arginine facilitates making a nucleosome receptive, in effect lowering the values of s and k to $s = 6$ and $k = 2$.

Under these conditions, we simulate the acetylation of a 4×4 solenoid graph as shown in Fig. 2d. The mean shortest path length for several probabilities of acetylation p are calculated and plot in Fig. 4a. Once p surpasses an apparent threshold, the mean shortest path length quickly shifts from its minimum value to its maximum value. Hence, we expect that the chromatin will exhibit some degree of bimodality as the conditions for p vary.

To describe the relationship between mean shortest path length and chromatin accessibility, notice that more nucleosome interactions generally lead to less chromatin accessibility. But chromatin accessibility is not merely determined by the number of interactions, since interactions could be clustered around a single small region of the DNA. A better measure of how accessible the DNA is would include the number of interactions as well as their distribution, which is described by the graph diameter. Also, if the nodes of a given 2D interaction graph were allowed to expand by diffusion, the graph diameter would indicate how widely the graph can spread. This is similar to the situation in the chromatin, which is constantly subject to diffusion by Brownian motion.

Following the reasoning above, we can provide a formula to calculate the accessibility of the chromatin by transcriptional enzymes using the mean shortest path lengths. First, note that, for $p = 0$, the shortest path length is equal to 5 as shown in Fig. 4a. This corresponds to chromatin that is fully compact and has interactions between all nucleosome neighbors. This chromatin has minimal accessibility and we can assign it a value of 0 to denote this. We assume a linear mapping between mean shortest path length and chromatin accessibility, and we derive a relationship between them as follows. Let M be the mean diameter (that is the mean shortest path length), M_0 the minimum diameter,

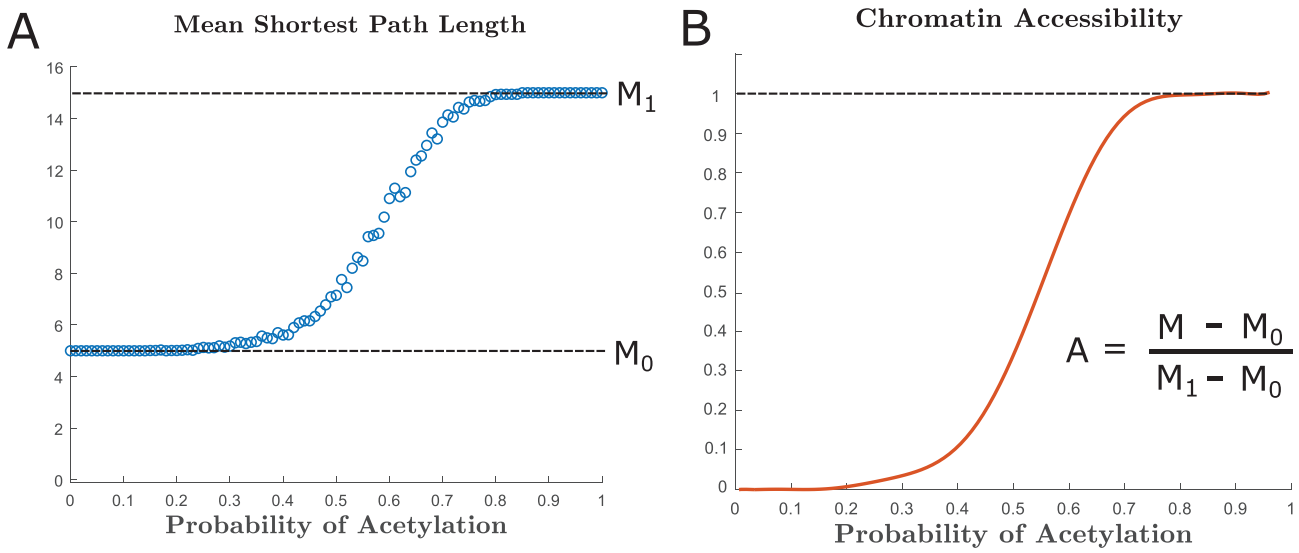

Fig. 4. The mean shortest path length is calculated as a function of the acetylation probability p using a 4×4 solenoid DNA structure as in Fig. 2d. Mean shortest path lengths were calculated from 100 independent simulations for each value of p, and this data was fitted with a polynomial function. Chromatin accessibility was estimated by vertical translation of this graph.

and M_1 the maximum diameter. Then the chromatin accessibility A can be described with the formula $A = (M - M_0)/(M_1 - M_0)$. This amounts to vertically translating and normalizing the mean shortest path length graph in Fig. 4a. The resulting graph in Fig. 4b shows chromatin that has an accessibility range from 0 (minimally accessible) to 1 (fully accessible) when $p = 0$ and $p = 1$, respectively.

4. Results

4.1. Spatially-bounded chromatin density regions

To understand the range of acetylation for HAT proteins, we refer to work by Vignali et al. (2000) which studied the SAGA and NuA4 HATs found in *Saccharomyces cerevisiae*. They consider an *in vitro* assay with DNA bound to unacetylated histones, which they stimulate with HAT molecules. They show that HAT proteins only operate in the presence of transcription factors such as Gal4-VP16. In order to determine the location and extent of histone acetylation along the DNA, they use a ChIP assay with antibodies specific to acetylated histones.

Importantly, they found that stimulation by transcription factor Gal4-VP16 results in characteristic distributions of acetylated histones, i.e., that SAGA and NuA4 acetylate the nucleosomes in their vicinity with differing probabilities (Fig. 5a). In the case of SAGA, the probability of acetylation decreases as the distance from the HAT binding site increases. We can use this information together with the data in Fig. 4b in order to calculate the chromatin accessibility as a function of base pair location (Fig. 5b). To do this, we simply compose the probability of acetylation for SAGA in Fig. 5a with the function in Fig. 4b. In other words, letting chromatin accessibility in Fig. 4b be denoted by $f(p)$ and the probability of acetylation p be given by Fig. 5a such that $p = g(b)$ for any base pair location b. Then, Fig. 5b would be given by $f(g(b))$.

The ultrasensitivity of the function in Fig. 4b is conserved in this composition where it creates sharp boundaries between regions of heterochromatin and euchromatin. These results suggest how a single HAT can decompress a region of the chromatin while maintaining sharp boundaries in accessibility between chromatin regions. Such accessibility peaks have been recorded experimentally under certain conditions and the ranges of chromatin expansion are similar to that of our simulated data (Wang et al., 2020). An example of this behavior is shown in Fig. 5c from Wang et al. (2020). This study performed ATAC-seq on cells from APP/PS1 mice models to measure their chromatin accessibility. The resulting average peaks happen to also be approximately 2000 bp long and in some cases define clear regions of expansion with sharp boundaries.

Whenever multiple transcription factor binding sites are present, a histone site can potentially be acetylated by one of multiple SAGA proteins. In order to model the effect of multiple sites interacting with each other, we make the assumption that each bound SAGA acts upon histones independently of other bound SAGA proteins. Given three separate binding sites, the probability of a histone site being acetylated by at least one of the three bound SAGA proteins is equal to $1 - (1 - p_1)(1 - p_2)(1 - p_3)$, where $p_i = g_i(b)$ corresponds to the probability of being acetylated by the SAGA protein at the i-th binding site (Fig. 5d). Moreover, when multiple SAGA are bound, a larger region of the chromatin can be decompressed. Specifically, the accessibility is now given by $f(1 - (1 - g_1(b))(1 - g_2(b))(1 - g_3(b)))$. If transcription factor binding sites are not too far apart, then a large single region is created that has consistently high accessibility and a sharp boundary with the rest of the chromatin (Fig. 5e). Each of the functions in this figure is calculated by composing the corresponding function in Fig. 5d with the function f above.

4.2. Chemical reaction network

To estimate the probability p of histone acetylation as a function of transcription factor concentrations, we construct a chemical reaction network that describes a simplified version of this process. Denote T to be an abstract representation of a transcription factor. T binds to a piece of DNA denoted by D to form complex C_1. Once C_1 is present, it proceeds to recruit a HAT (denoted by H) and forms complex C_2. A non-acetylated histone site S can be acetylated into A by interacting with C_2. Acetylated sites spontaneously go back to being non-acetylated at a fixed rate, in effect by assuming a constant background amount of histone deacetylase (HDAC) that is not explicitly modeled in this system. The reaction network can be summarized as in Fig. 6a.

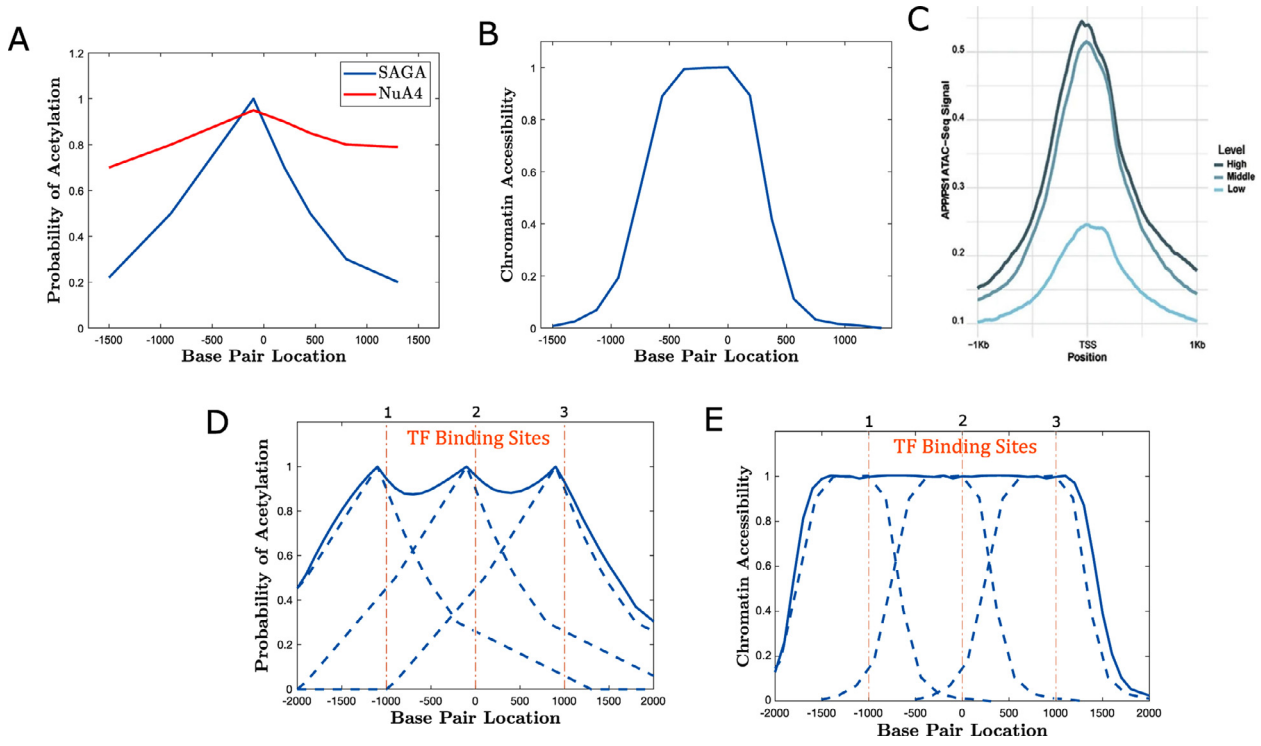

Fig. 5. (A) Data from Vignali et al. (2000) showing the percentage of acetylated histones at each base pair location relative to the binding site of the SAGA and NuA4 HAT proteins. (B) Chromatin accessibility calculated from a single bound SAGA protein as a function of base pair location, using (A) and the accessibility data from Fig. 4b. (C) ATAC-seq data from APP/PS1 mice as part of an analysis on chromatin accessibility in Alzheimer's disease (Wang et al., 2020). (D) Probability of being acetylated by at least one of three bound SAGA proteins at a given base pair location (solid line). The probabilities of acetylation from individual SAGA proteins are marked in dashed lines. Binding sites are separated by 1000 base pairs each. (E) Levels of chromatin accessibility resulting from three bound SAGA proteins (solid line), calculated using data from (D) and Fig. 4b. Levels of accessibility resulting from individual bound SAGA proteins are marked usi.ng dashed lines.

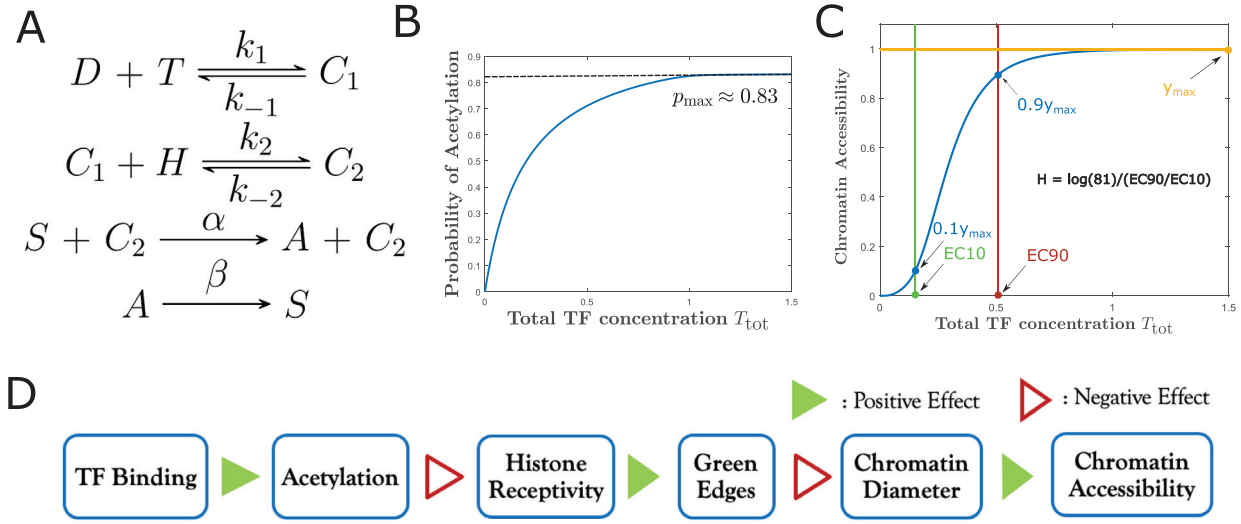

Fig. 6. (A) Chemical reactions describing HAT forming a complex with DNA and transcription factor, and reversible histone acetylation. (B) Probability of acetylation p calculated as a function of total TF concentration T_{tot}. (C) Modeled relationship between total transcription factor and levels of chromatin expansion, using (A) and data from Fig. 4b. Here $k_1 = 1, k_2 = 1, \alpha = 1, k_{-1} = 0.2, k_{-2} = 0.2, \beta = 0.2, D_{\text{tot}} = 1, H_{\text{tot}} = 16, D_0 = D_{\text{tot}}, S_0 = S_{\text{tot}}, H_0 = H_{\text{tot}}$, and $T_0 = T_{\text{tot}}$. (D) Summary diagram of the different variables involved in the model, from transcription factor binding input to chromatin accessibility output.

This system uses kinetic rate parameters $k_1, k_2, k_{-1}, k_{-2}, \alpha, \beta$ as described in the reactions, with values shown in the Methods section. The system also has total protein concentrations which do not change over time, such as the total concentration of histone sites $S_{\text{tot}} = S + A$ and the total transcription factor $T_{\to t} = T + C_1 + C_2$, as well as $D_{\to t}$ and $H_{\to t}$.

We model this system deterministically using mass action kinetics (Chellaboina et al., 2009). Under nonzero initial conditions,

the network eventually converges to a steady state of nonzero acetylated and nonzero non-acetylated histone sites. Therefore, we can calculate the probability of acetylation for a histone site. First, we compute the steady state of acetylated sites which turns out to be

$$A = \frac{S_{\text{tot}} k_1 k_2 \alpha DTH}{k_1 k_2 \alpha DTH + k_{-1} k_{-2} \beta} = \frac{S_{tot} DTH}{DTH + K},$$

where $K = k_{-1}k_{-2}\beta/(k_1 k_2 \alpha)$. Then, dividing A by the total number of sites S_{tot} yields the probability of acetylation at the steady state

$$p = \frac{A}{S_{\text{tot}}}. \tag{2}$$

We will calculate the value of p as a function of total concentrations and rate parameters in Section 4.3. See the Supplementary Material for an explicit calculation.

4.3. Ultrasensitive chromatin remodeling

Using the chemical reaction formalism above, we can now write the probability of acetylation as a function of total transcription factor concentration. It is important to note that even when transcription factor is bound with very high frequency, the probability of acetylation depends on the balance between histone acetylation and histone deacetylation. In other words, in the limit as T_{tot} increases, the probability of acetylation does *not* converge to 1 in this system. If the value of p remains low even for very large T_{tot}, then chromatin will never decompress per Fig. 4b.

In particular, whenever there is saturation of T and H, the values of D and C_1 become small enough so that $C_2 = D_{tot}$ and our chemical reaction network reduces to

$$S \underset{\beta}{\overset{D_{\text{tot}}\alpha}{\rightleftharpoons}} A.$$

Since there is a limited number of binding sites in a given chromatin region, we can expect that D_{tot} is small, and we set for simplicity $D_{\text{tot}} = 1$. Then, the steady of state of A at saturation of T and H can be written as

$$A_{\text{sat}} = \frac{S_{\text{tot}} D_{\text{tot}} \alpha}{D_{\text{tot}} \alpha + \beta} = \frac{S_{\text{tot}} \alpha}{\alpha + \beta}. \tag{3}$$

It is clear that, under these conditions, the rate of acetylation α, the rate of deacetylation β, and the total number of sites S_{tot} play the only role in determining the number of acetylated sites at steady state. Since $p_{\max} = A_{\text{sat}}/S_{\text{tot}}$, then α and β determine maximum value of p when T and H are saturated. From this, we can choose $\alpha = 1$ and $\beta = 0.2$ to obtain $p_{\max} = 1/(1 + 0.2) \approx 0.83$. Under a fixed large value of H, p takes the shape in Fig. 6b which in the limit of T_{tot} approximates our calculation of $p_{\max} \approx 0.83$ (see Methods for the other parameter choices). A large value of $p_{\max}$ implies that, for the function in Fig. 4b, the chromatin will decompress for a large enough T_{tot}.

To determine ultrasensitivity of the mean shortest path length with respect to T_{tot}, we compose the functions in Figs. 4b and 6b. The plot in Fig. 6c shows an apparent ultrasensitive dose–response between total transcription factor concentration and chromatin expansion. To quantify these levels of ultrasensitivity, we use the Hill coefficient which in the case of Hill functions $x^n/(x^n + c)$ corresponds to the parameter n. The higher the value of n, the more ultrasensitive this function becomes. For general functions, such as that in Fig. 6c, we can use the generalized definition of the Hill coefficient derived by Goldbeter and Koshland (Goldbeter and Koshland, 1981; Enciso, 2102) with the formula $H = \log(81)/(\log(EC90/EC10))$. Here EC10 and EC90 refer to the input concentrations that produce 10% and 90% of the maximal response, respectively. It can be shown that applying this formula to the function $x^n/(x^n + c)$, one obtains the original Hill coefficient n.

The Hill coefficient of the function in Fig. 6c was calculated to be 3.7. Typically, Hill coefficients above 2 are characteristic of ultrasensitive responses (Koshland et al., 1982). This confirms that our modeled chromatin can give rise to ultrasensitive responses, thus preventing state transitions until a critical concentration of transcription factors is present.

To recapitulate how we arrived at this result, we summarize the entire process of acetylation leading to chromatin remodeling, which is also outlined in Fig. 6d. First, for a given transcription factor concentration, determine the probability of acetylation using the given chemical reaction network (Fig. 6a). This probability p is then used to calculate the probability that a nucleosome will be receptive in the chromatin graph (1). If two neighboring nucleosomes are receptive, then a green edge corresponding to a nucleosomal interaction should be added between them. This yields a chromatin graph as those in Fig. 2b from which a shortest path and associated chromatin accessibility can be derived. Repeating these steps for different amounts of T_{tot} ultimately gives a graph similar to the one in Fig. 6c and the ultrasensitivity of the chromatin remodeling can be measured by taking the Hill coefficient of this graph.

4.4. Effects of s,k, and graph sizes on Hill coefficients

We determine the sensitivity of the Hill coefficient to different parameter values by running multiple additional simulations. The parameters that we vary include the number of rows and columns of the DNA interaction grid, as well as the parameters s, k that determine the nucleosomal interactions.

We first choose a large value of α relative to β and use Eq. (3) to obtain a $p_{\max}$ large enough that it guarantees full chromatin decompression for all values of s and k in our chosen range (Fig. 7b). The resulting Hill coefficients for each combination of s and k are displayed as a heat map shown in Fig. 7a. In this case, Hill coefficients are maximized whenever $k \approx s/2$, with $H > 4$ for $s = 10, k = 6$. This suggests that ultrasensitivity in chromatin remodeling can be maximized by having twice as many sites than the minimum number of non-acetylated sites required for nucleosome interactions.

For lower values of $p_{\max}$, the chromatin may not fully decompress for some combinations of s and k (Fig. 7d). Hill coefficients appear to be maximized for large values of s and small values of k (Fig. 7c), with $H > 4.5$ for $s = 10, k = 2$. In this case the maximal DNA accessibility reaches around 40% of the full expansion. This illustrates a parameter regime in which a dose response of chromatin expansion is highly ultrasensitive, even though chromatin is never fully expanded.

We note that these heat maps also separate between the effect of percolation and the nucleosomal interactions to determine the Hill coefficient. Specifically, when $s = k = 1$ in Fig. 7c, nucleosomal interactions are simplified and $H \approx 2$ in the solenoid model.

In the same manner as with s and k, we simulate chromatin graphs with different row and column numbers. The Hill coefficients for the solenoid and interdigitation graphs of different sizes are calculated and shown as heat maps in Figs. 8a and 8b respectively. For the solenoid architecture, the trend appears to be that increasing the number of rows and columns increases the ultrasensitivity of the response. Note that, in three dimensions, the number of columns could be interpreted as the magnitude of the solenoid radius. Interdigitation architectures, however, tend to become more ultrasensitive solely with increases in the number of

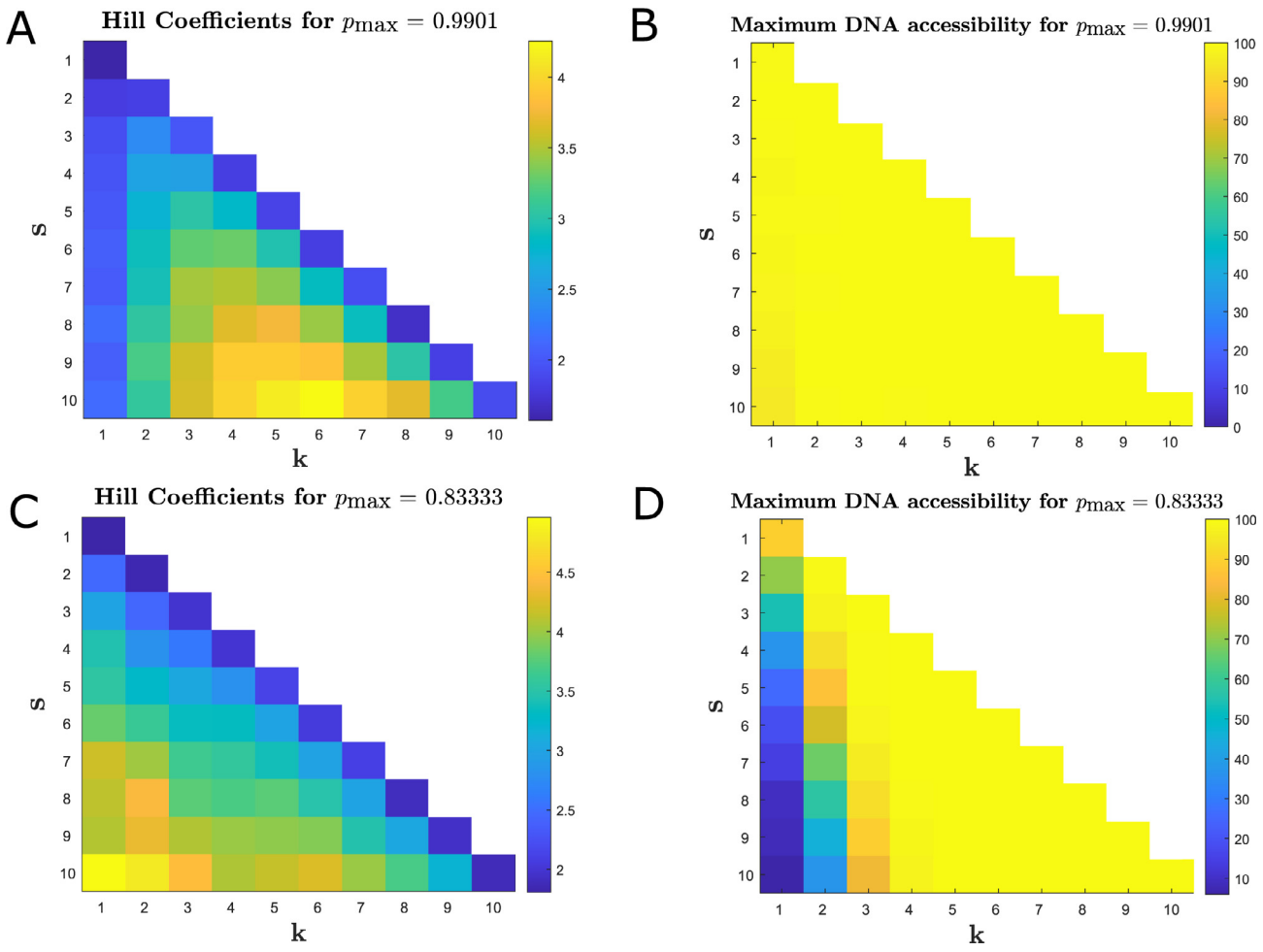

Fig. 7. (A) In a parameter regime where the probability of acetylation p saturates as a function of T_{tot}, the Hill coefficient can be higher than 4 for certain combinations of s, k. (B) Using the same parameters as in (A), DNA accessibility saturates near 100% for most values of s, k. (C) If the probability of acetylation doesn't fully saturate, the maximum Hill coefficient of approximately 4 is found for small k and high s. (D) Using the same parameters, the values of s, k that optimize ultrasensitivity have low saturation of DNA accessibility. That is, the DNA response is ultrasensitive but it never fully opens for increasing TF concentration. For subfigures (C) and (D) we used the same parameters as in Fig. 6. Similarly for (A) and (B) with the exception of $k_{-1} = 10^{-2}, k_{-2} = 10^{-2}$ and $\beta = 10^{-2}$, we use the .same parameters.

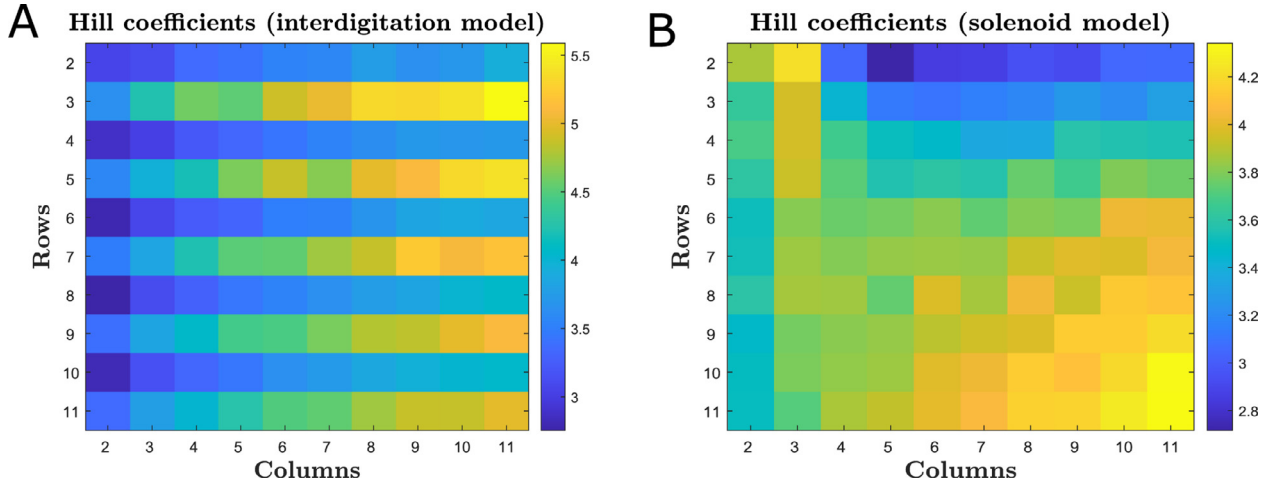

Fig. 8. (A) Hill coefficients for different grid sizes of the solenoid model. Higher numbers of rows and columns tend to increase the ultrasensitivity of the transcription factor dose–response. (B) Hill coefficients for different grid sizes of the interdigitation model. Higher numbers of columns raise the ultrasensitivity of the transcription factor dose–response. Parameters were chosen as in Fig.. 7a.

columns. Here, more columns correspond to longer stretches of the chromatin before each fold in the architecture. Notice also that even numbers of rows tend to lead to very low Hill coefficients regardless of the number of columns. We believe this to be an artifact, since in this case the end points of the DNA are located in the same column.

5. Comparison with experimental results

Experimental work by Hajihassan and collaborators measured ultrasensitive chromatin aggregation in response to increasing concentrations of the anticancer drug mitoxantrone (Hajihassan and Rabbani-Chadegani, 2009). This drug is believed to bind to histones and DNA and to prevent the activity of HAT enzymes, leading to higher chromatin density. We postulate that the ultrasensitive behavior they found could be due to the percolation effects described in our work, and we have recapitulated their experimental data using an expanded model of histone acetylation.

Hajihassan et al. created an *in vitro* extract of rat liver cell chromatin, and they measured chromatin aggregation under different concentrations of mitoxantrone. Chromatin aggregation was measured indirectly by determining the light absorbance of the solution at 400 nm frequency, which is known to measure the turbidity of a solution. In the words of Hajihassan et al., "Addition of drug to SE-chromatin solution resulted in chromatin aggregation and precipitation which could be detected by monitoring the absorbance at 400 nm (turbidity)." The authors found a dose–response between turbidity and mitoxantrone concentration with a Hill coefficient of approximately 3.6. They conclude that the binding of the drug to DNA is likely cooperative, however we postulate here a possible alternative explanation.

The ability of mitoxantrone to inhibit HAT in a dose-dependent manner has been previously documented (Khan et al., 2011). We incorporated mitoxantrone into our chemical reaction system by assuming that it binds to the HAT-DNA complex, forming a new complex in which HAT is inactive (Fig. 9a). In this way, mitoxantrone reduces overall levels of histone acetylation, which decreases chromatin accessibility in an ultrasensitive manner.

In Fig. 9b, we calculate overall levels of histone acetylation and chromatin accessibility for different drug concentrations. In order to quantitatively relate chromatin accessibility with normalized turbidity data, we assume a simple linear relationship $\textit{turbidity} = 1 - \textit{accessibility}$. Using this relationship we are able to recapitulate the experimental measurement using our model, and we show that it displays a similar ultrasensitive behavior with a simulated Hill coefficient of approximately 3.8 (Fig. 9c).

6. Discussion

We develop a theoretical model that uses ideas from percolation theory and nonessential modification sites in order to create ultrasensitive regulation of chromatin expansion. This regulation is naturally limited to the regions of transcription factor binding and is not based on cooperativity of histone acetylation. This results in sharp spatial boundaries between low and high density regions and ultrasensitive chromatin decompaction in response to HAT-recruiting transcription factors. Further analysis shows the effect that changing the DNA configuration has in the resulting ultrasensitive behavior. In particular, wide and/or long DNA solenoids have greater Hill coefficients, as do interdigitation structures with long DNA stretches between folds.

Overall, our work describes a mechanism for how chromatin accessibility may be able to respond in an all-or-none manner to the acetylation of histone sites. This response could be explored experimentally with a ChIP-seq assay to measure the fraction of acetylated histone sites in a particular chromatin region. Chromatin accessibility, in turn, could be approximated using ATAC-seq, by proxy through gene expression levels, or through direct inspection using electron microscopy. These experiments are out of the scope of this paper and are left for a future publication, for instance using the ENCODE database and comparing data for single cells or tissues using different assays. We have also predicted a relation between DNA structure and Hill coefficient which could be tested experimentally.

The ultrasensitive behavior in our model is due in part to a proposed mechanism in which a critical mass of acetylations between two neighboring histones are required before the histones alter the interaction with each other and the underlying DNA. Previous modeling and experimental results show that this critical mass is ideally less than the total number of acetylation sites, leading to the concept of *nonessential* sites. Overall, our results suggest that chromatin features that appear nonessential could play a role in the context of ultrasensitive remodeling.

An expanded version of our model was able to account for experimental data using an anticancer drug measured by Hajihassan and collaborators (Hajihassan and Rabbani-Chadegani, 2009). While the actual mechanism for the observed ultrasensitivity is not yet determined, one possibility is that it may be due to percolation effects and nonessential interaction histone sites.

In summary, the model calculates the steady state probability p that a histone will be modified and determines the presence of green edges corresponding to nucleosomal interactions. The shortest path of the resulting chromatin graph is used to calculate the chromatin accessibility, which will have different values for different amounts of T_{tot}. This yields the dose response of chromatin accessibility as a function of local transcription factor concentration. The Hill coefficient of this graph represents the level of ultrasensitivity at which the chromatin transitions between density states.

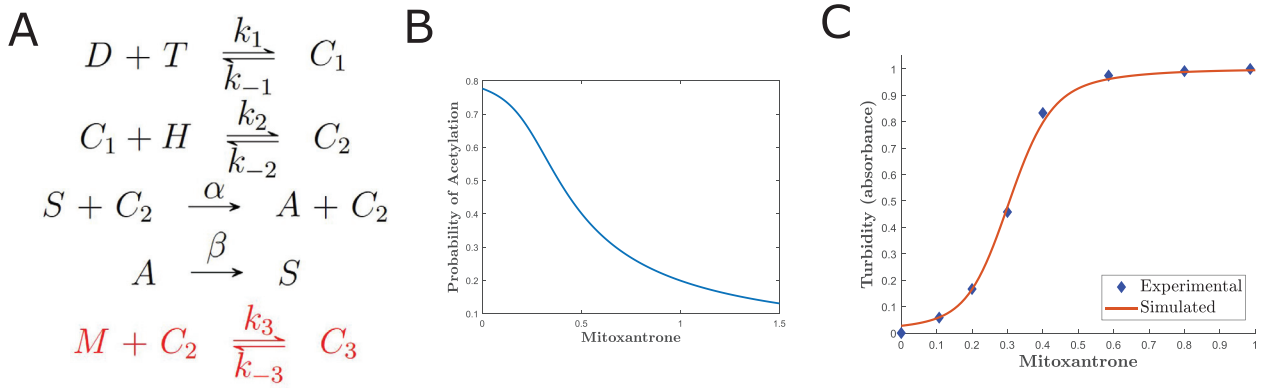

Fig. 9. (A) Expanded chemical reaction network including reversible enzyme inactivation through mitoxantrone binding to the DNA-HAT complex, forming a new complex C_3. (B) Simulated probability of acetylation p calculated as a function of total mitoxantrone concentration. (C) Experimental data of chromatin turbidity as a function of mitoxantrone concentration along with the modeled relationship between using (A) and data from Fig. 4b. Here $k_1 = 0.0005, k_2 = 0.031, \alpha = 1.5$, $k_{-1} = 1.5, k_{-2} = 0.18$, $\beta = 0.02, k_3 = 1.5, k_{-3} = 0.0001$, $D_{\text{tot}} = 1, H_{\text{tot}} = 16, T_{\text{tot}} = 50, D_0 = D_{\text{tot}}, S_0 = S_{\text{tot}}$, $H_0 = H_{\text{tot}}, T_0 = T_{\text{tot}}$, and $M_0 = M_{\text{tot}}$.

A future version of this model could incorporate additional factors that can be biologically relevant. Perhaps most immediately, the effects of methylation could be incorporated. Methylation is a covalent modification that prevents acetylation of a given amino acid, and it therefore blocks DNA expansion. It is often used to silence blocks of DNA in the genome. In the context of our work, one could include methylation simply by adding methylation reactions $S \Longleftrightarrow M$ to the chemical reaction network, with the forward reaction mediated by an appropriate HMT enzyme.

While we include nucleosome modifications in the model, we do not include the possibility of nucleosome eviction from the DNA, which would likely alter DNA configuration. Also, additional DNA interactions resulting from higher order three-dimensional folds may result in new neighbors between nucleosomes and can be included by adding interactions to the 2D structure graph. Other factors that are known to play a role in chromatin remodeling are the topology of linker DNA, and the presence of proteins such as the H1 linker histone.

Credit authorship contribution statement

Alvaro Fletcher: Conceptualization, Formal analysis, Investigation, Methodology, Software, Writing – original draft, Writing – review & editing. **Ruonan Zhao:** Formal-analysis, Investigation, Methodology, Software, Visualization, Writing-review-editing. **German Enciso:** Conceptualization, Formal-analysis, Funding-acquisition, Project-administration, Supervision, Writing-review-editing.

Declaration of Competing Interest

The authors declare that they have no known competing financial interests or personal relationships that could have appeared to influence the work reported in this paper.

Acknowledgements

We would like to thank Juan Manuel Pedraza and Jun Allard for insights regarding this work. All authors were partially supported by NSF grant DMS1763272, Simons Foundation grant 594598 (Qing Nie) and by NSF grant DMS1616233.

Appendix A: The probability p as a function of total concentrations and rate parameters

We wish to show that p in Eq. (2) depends only on rate constants and total concentrations. First note that the chemical reaction network in Section 4.2 can be written by mass-action kinetics as

$$\begin{cases} \frac{dT}{dt} &= k_{-1}C_1 - k_1 DT \\ \frac{dD}{dt} &= k_{-1}C_1 - k_1 DT \\ \frac{dC_1}{dt} &= k_1 DT - k_{-1}C_1 - k_2 C_1 H + k_{-2}C_2 \\ \frac{dC_2}{dt} &= k_2 C_1 H - k_{-2}C_2 \\ \frac{dS}{dt} &= \beta A - \alpha S C_2 \\ T_{\text{tot}} &= T + C_1 + C_2 \\ D_{\text{tot}} &= D + C_1 + C_2 \\ H_{\text{tot}} &= H + C_2 \\ S_{tot} &= S + A \end{cases} \tag{A.1}$$

At steady state,

$$\begin{cases} k_1 DT &= k_{-1}C_1 \\ k_2 C_1 H &= k_{-2}C_2 \\ \beta A &= \alpha S C_2 \end{cases} \quad \text{or} \quad \begin{cases} K_1 DT &= C_1 \\ K_2 C_1 H &= C_2 \\ K_3 S C_2 &= A \end{cases},$$

where $K_1 = k_1/k_{-1}, K_2 = k_2/k_{-2}$, and $K_3 = \alpha/\beta$. By mass conservation laws in (A.1),

$$\begin{aligned} D &= D_{\text{tot}} - (C_1 + C_2) \\ &= D_{\text{tot}} - (T_{\text{tot}} - T) \\ &= T - Q_1, \end{aligned} \tag{A.2}$$

where $Q_1 = T_{\text{tot}} - D_{\text{tot}}$. We can then perform the appropriate substitutions in the expression for T_{tot} to obtain

$$\begin{aligned} T_{\text{tot}} &= T + C_1 + C_2 \\ &= T + K_1 DT + K_2 K_1 DTH. \end{aligned} \tag{A.3}$$

If $C_2 \leqslant D_{\text{tot}}$ and $D_{\text{tot}} \ll H_{\text{tot}}$, then $C_2 \ll H_{\text{tot}}$ and thus

$H = H_{\text{tot}} - C_2 \approx H_{\text{tot}}$.

Then, by (A.3),

$$\frac{T_{\text{tot}}}{T} \approx 1 + D(K_1 + K_1 K_2 H_{\text{tot}}) = 1 + (K_1 + K_1 K_2 H_{\text{tot}})(T - Q_1). \tag{A.4}$$

Let $f_1(T) = T_{\text{tot}}/T$, and $f_2(T) = 1 + (K_1 + K_1 K_2 H_{\text{tot}})(T - Q_1)$. We show that there is a unique positive solution for T in (A.4).

First note that f_1 is a decreasing function for $T > 0$. Also, the function f_2 is a straight line with slope $K_1 + K_1 K_2 H_{\text{tot}} > 0$. Therefore, f_1 and f_2 have a single intersection which corresponds to a unique, positive solution for T. From Eq. (A.4), we can write

$$(K_1 + K_1 K_2 H_{\text{tot}})T^2 + (1 - K_1 - K_1 K_2 H_{\text{tot}})Q_1 T - T_{\text{tot}} = 0,$$

and solving for T yields

$$T = \frac{((K_1 + K_1 K_2 H_{\text{tot}}) - 1)Q_1 \pm \sqrt{(1 - (K_1 + K_1 K_2 H_{\text{tot}}))^2 Q_1^2 + 4(K_1 + K_1 K_2 H_{\text{tot}})T_{\text{tot}}}}{2(K_1 + K_1 K_2 H_{\text{tot}})}.$$

Since T has a unique, positive solution and

$$\begin{aligned} ((K_1 + K_1 K_2 H_{\text{tot}}) - 1)Q_1 &\leqslant |((K_1 + K_1 K_2 H_{\text{tot}}) - 1)Q_1| \\ &= \sqrt{(((K_1 + K_1 K_2 H_{\text{tot}}) - 1)Q_1)^2} \\ &\leqslant \sqrt{(1 - (K_1 + K_1 K_2 H_{tot}))^2 Q_1^2 + 4((K_1 + K_1 K_2 H_{\text{tot}})T_{\text{tot}}}, \end{aligned}$$

then it must be that

$$T = \frac{((K_1 + K_1 K_2 H_{\text{tot}}) - 1)Q_1 + \sqrt{(1 - (K_1 + K_1 K_2 H_{\text{tot}}))^2 Q_1^2 + 4(K_1 + K_1 K_2 H_{tot})T_{\text{tot}}}}{2(K_1 + K_1 K_2 H_{\text{tot}})}.$$

Solving for A, we have that

$$A = K_3 S C_2 = K_3 K_2 C_1 H S = K_3 K_2 K_1 DTHS,$$

which implies

$$A = \frac{K_3 K_2 K_1 DTH_{\text{tot}} S_{\text{tot}}}{1 + K_3 K_2 K_1 DTH_{\text{tot}}} = \frac{\frac{\alpha}{\beta}\frac{k_2}{k_{-2}}\frac{k_1}{k_{-1}} DTHS_{tot}}{1 + \frac{\alpha}{\beta}\frac{k_2}{k_{-2}}\frac{k_1}{k_{-1}} DTH} = \frac{\alpha k_2 k_1 DTHS_{tot}}{\beta k_{-2} k_{-1} + \alpha k_2 k_1 DTH}.$$

Therefore,

$$p = \frac{A^*}{S_{tot}} = \frac{\alpha k_2 k_1 DTH}{\beta k_{-2} k_{-1} + \alpha k_2 k_1 DTH}.$$

By substituting the above expressions for $T, D = T - T_{\text{tot}} + D_{\text{tot}}$ and $H \approx H_{\text{tot}}$ into the equation for p, we can obtain p as a function of parameters $k_1, k_{-1}, k_2, k_{-2}, \alpha, \beta, H_{\text{tot}}, S_{\text{tot}}, T_{\text{tot}}$.

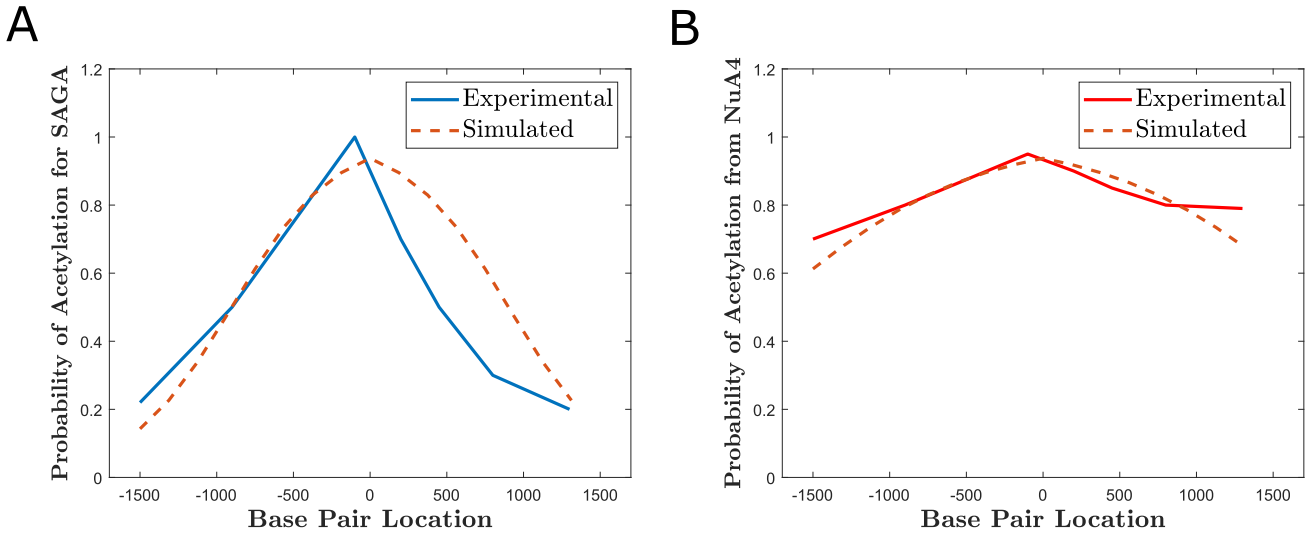

Fig. 10. Probabilities of acetylation with respect to base pair location for rates of acetylation α that decrease exponentially from the HAT binding site. Under these conditions, simulated HAT acetylation profiles can be made to resemble their experimental counterparts. Different exponential rates were enough to account for the differences between the SAGA and NuA4 acetylation profiles. Simulations were done for 16 nucleosomes (each with 8 sites). Parameters were chosen as $D_{\text{tot}} = 1, T_{\text{tot}} = 1.5$, $H_{\text{tot}} = 16, k_1 = 5, k_2 = 5$, $k_{-1} = 1, k_{-2} = 1$, and $\beta = 1$. The values of α in Eq. (B.5) were given by $\alpha_0 = 25$ with values for c equal to 0.003 and 0.0015 for SAGA and NuA4 respectively. Initial conditions were set to $D = D_{\text{tot}}, S_0 = S_{\text{tot}}$, $H_0 = H_{\text{tot}}$, and $T_0 = .T_{\text{tot}}$.

Appendix B: Simulated HAT acetylation ranges

Recall that the rate α in our chemical reaction network describes the rate at which sites become acetylated. To replicate the experimentally measured acetylation profiles for the SAGA and NuA4 HAT proteins, we assumed that α decreases exponentially as a function of the distance from the HAT binding site. In particular we set

$$\alpha = \alpha_0 e^{-c|b|}, \tag{B.5}$$

where α_0 is the maximum value of α, c is a constant, and b is base pair location. The probability of acetylation p in Eq. 2 can then be calculated as a function of base pair location by appropriately changing the value of α. Plotting these values of p yields simulated acetylation profiles that resemble their experimental counterparts for SAGA and NuA4 (Fig. 10a and b).

References

Bannister, Andrew J., Kouzarides, Tony, 2011. Regulation of chromatin by histone modifications. Cell Res. 21, 381–395. https://doi.org/10.1038/cr.2011.22.

Barnes, Claire E., English, David M., Cowley, Shaun M., 2019. Acetylation & Co: an expanding repertoire of histone acylations regulates chromatin and transcription. Essays Biochem. 63(1). Ed. by Nick Gilbert and James Allan, pp. 97–107. issn: 0071-1365, 1744-1358. doi: 10.1042/EBC20180061. url: https://portlandpress.com/essaysbiochem/article/63/1/97/166/Acetylation-amp-Co-an-expanding-repertoire-of (visited on 07/24/2021)..

Chellaboina, Vijaysekhar et al., 2009. Modeling and analysis of mass-action kinetics. IEEE Control Syst. Mag. 29 (4), 60–78.

Cormen, Thomas H., et al. Introduction to Algorithms. third ed. pp. 658–662. isbn:9780262033848..

Dodd, Ian B., Sneppen, Kim, 2011. Barriers and silencers: A theoretical toolkit for control and containment of nucleosome-based epigenetic states. J. Mol. Biol. 414 (4), 624–637. https://doi.org/10.1016/j.jmb.2011.10.027.

Durrin, Linda K. et al., 1991. Yeast histone H4 N-terminal sequence is required for promoter activation in vivo. Cell 65 (6), 1023–1031. https://doi.org/10.1016/0092-8674(91)90554-C. ISSN: 00928674. URL: https://linkinghub.elsevier.com/retrieve/pii/009286749190554C (visited on 07/24/2021).

Enciso, Germán A., 2013. Multisite Mechanisms for Ultrasensitivity in Signal Transduction. In: Kloeden P., Pötzsche C. (eds) Nonautonomous Dynamical Systems in the Life Sciences. Lecture Notes in Mathematics. Springer, Cham 2102..

Erdel, Fabian, Greene, Eric C., 2016. Generalized nucleation and looping model for epigenetic memory of histone modifications. Proc. Natl. Acad. Sci. 113 (29), E4180–E4189. https://doi.org/10.1073/pnas.1605862113. ISSN: 0027-8424 1091-6490.

Felsenfeld, Gary, McGhee, James D., 1986. Structure of the 30 nm chromatin fiber. Cell 44 (3), 375–377. https://doi.org/10.1016/0092-8674(86)90456-3.

Finch, J.T., Klug, A., 1976. Solenoidal model for superstructure in chromatin. Proc. Natl. Acad. Sci. U.S.A. 73 (6), 1897–1901. https://doi.org/10.1073/pnas.73.6.1897.

Fry, Christopher J., Peterson, Craig L., 2001. Chromatin remodeling enzymes: who's on first? Curr. Biol. 11 (5), R185–197. https://doi.org/10.1016/s0960-9822(01)00090-2.

Fussner, Eden et al., 2012. Open and closed domains in the mouse genome are configured as 10-nm chromatin fibres. EMBO Rep. 13 (11), 992–996. https://doi.org/10.1038/embor.2012.139.

Goldbeter, Albert, Koshland Jr, Daniel E., 1981. An amplified sensitivity arising from covalent modification in biological systems. Proc. Natl. Acad. Sci. U.S.A. 78 (11), 6840–6844.

Görisch, Sabine M. et al., 2005. Histone acetylation increases chromatin accessibility. J. Cell Sci. 118 (24), 5825–5834. https://doi.org/10.1242/jcs.02689.

Hajihassan, Zahra, Rabbani-Chadegani, Azra, 2009. Studies on the binding affinity of anticancer drug mitoxantrone to chromatin DNA and histone proteins. J. Biomed. Sci. 16 (1), 1–7. https://doi.org/10.1186/1423-0127-16-31.

Hodges, C., Crabtree, G.R., 2012. Dynamics of inherently bounded histone modification domains. Proc. Natl. Acad. Sci. 109 (33), 13296–13301. ISSN: 0027-8424.

Honda, Shinji et al., 2010. The DMM complex prevents spreading of DNA methylation from transposons to nearby genes in Neurospora crassa. Genes Develop. 24 (5), 443–454. https://doi.org/10.1101/gad.1893210.

Jost, Daniel, Vaillant, Cédric, 2018. Epigenomics in 3D: importance of long-range spreading and specific interactions in epigenomic maintenance. Nucl. Acids Res. 46 (5), 2252–2264. https://doi.org/10.1093/nar/gky009. ISSN: 0305-1048, 1362-4962.

Kan, P.Y., Caterino, T.L., Hayes, J.J., 2009. The H4 Tail Domain Participates in Intra- and Internucleosome Interactions with Protein and DNA during Folding and Oligomerization of Nucleosome Arrays. Mol. Cell. Biol. 29 (2), 538–546. https://doi.org/10.1128/mcb.01343-08.

Khan, Shahper N. et al., 2011. Mitoxantrone Induced Impediment of Histone Acetylation and Structural Flexibility of the Protein. Cell Biochem. Biophys. 60 (3), 209–218. https://doi.org/10.1007/s12013-010-9141-9.

Koshland, Daniel E., Goldbeter, Albert, Stock, Jeffry B., 1982. Amplification and Adaptation in Regulatory and Sensory Systems. Science 217 (4556), 220–225. https://doi.org/10.1126/science.7089556.

Krajewski, Wladyslaw A., 2016. "On the role of inter-nucleosomal interactions and intrinsic nucleosome dynamics in chromatin function. Biochem. Biophys. Rep. 5, 492–501. https://doi.org/10.1016/j.bbrep.2016.02.009.

Kulaeva, Olga I. et al., 2012. Internucleosomal interactions mediated by histone tails allow distant communication in chromatin. J. Biol. Chem. 287 (24), 20248–20257. https://doi.org/10.1074/jbc.M111.333104.

Kurdistani, Siavash K., Tavazoie, Saeed, Grunstein, Michael, 2004. Mapping Global Histone Acetylation Patterns to Gene Expression. Cell 117 (6), 721–733. https://doi.org/10.1016/j.cell.2004.05.023. ISSN: 00928674. URL: https://linkinghub.elsevier.com/retrieve/pii/S0092867404005367 (visited on 07/23/2021).

Lee, Ju Yeon, Wei, Sijie, Lee, Tae Hee, 2011. Effects of histone acetylation by Piccolo NuA4 on the structure of a nucleosome and the interactions between two

nucleosomes. J. Biol. Chem. 286 (13), 11099–11109. https://doi.org/10.1074/jbc.M110.192047.
Legube, Gaëlle, Trouche, Didier, 2003. Regulating histone acetyltransferases and deacety617 lases. EMBO Rep. 4 (10), 944–947. https://doi.org/10.1038/sj.embor.embor941.
Li, Zhenhai, Kono, Hidetoshi, 2016. Distinct Roles of Histone H3 and H2A Tails in Nucleosome Stability. Scientific Rep. 6 (31437), 1–12. https://doi.org/10.1038/srep31437.
Li, Guangyao, Zhou, Lei, 2013. Genome-Wide Identification of Chromatin Transitional Regions Reveals Diverse Mechanisms Defining the Boundary of Facultative Heterochromatin. PLoS One 8 (6). https://doi.org/10.1371/journal.pone.0067156.
Maeshima, Kazuhiro et al., 2014. Chromatin as dynamic 10-nm fibers. Chromosoma 123 (3), 225–237. https://doi.org/10.1007/s00412-014-0460-2.
Maeshima, Kazuhiro, Hihara, Saera, Eltsov, Mikhail, 2010. Chromatin structure: does the 30-nm fibre exist in vivo? Curr. Opin. Cell Biol. 22 (3), 291–297. https://doi.org/10.1016/j.ceb.2010.03.001. ISSN: 09550674. URL: https://linkinghub.elsevier.com/retrieve/pii/S0955067410000256 (visited on 07/25/2021).
Maeshima, Kazuhiro, Ide, Satoru, Babokhov, Michael, 2019. Dynamic chromatin organization without the 30-nm fiber. Curr. Opin. Cell Biol. 58 (30), 95–104. https://doi.org/10.1016/j.ceb.2019.02.003.
Marion, Christian, Roux, Bernard, 1980. Influence of histone H1 on chromatin structure. Biochem. Biophys. Res. Commun. 94 (2), 535–541. https://doi.org/10.1016/0006-291X(80)91264-4.
Marmorstein, Ronen, Roth, Sharon Y., 2001. Histone acetyltransferases: Function, structure, and catalysis. Curr. Opin. Genet. Develop. 11 (2), 155–161. https://doi.org/10.1016/S0959-437X(00)00173-8.
Michieletto, D., Orlandini, E., Marenduzzo, D., 2016. Polymer model with epigenetic recoloring reveals a pathway for the de novo establishment and 3D organization of chromatin domains. Phys. Rev. X 6 (4), 1–15. https://doi.org/10.1103/PhysRevX.6.041047. eprint: 1606.04653.
Mirny, Leonid A., 2010. Nucleosome-mediated cooperativity between transcription factors. Proc. Natl. Acad. Sci. U.S.A. 107 (52), 22534–22539. https://doi.org/10.1073/pnas.0913805107.
Mukhopadhyay, Swagatam, Sengupta, Anirvan M., 2013. The Role of Multiple Marks in Epigenetic Silencing and the Emergence of a Stable Bivalent Chromatin State. PLoS Comput. Biol. 9 (7). https://doi.org/10.1371/journal.pcbi.1003121. Ed. by Narendra Maheshri, e1003121. issn: 1553-7358.
Ou, Horng D. et al., 2017. ChromEMT: Visualizing 3D chromatin structure and compaction in interphase and mitotic cells. Science 357 (6349), eaag0025. https://doi.org/10.1126/science.aag0025. ISSN: 0036-8075, 1095-9203.
Pepenella, Sharon, Murphy, Kevin J., Hayes, Jeffrey J., 2014. Intra- and inter-nucleosome interactions of the core histone tail domains in higher-order chromatin structure. Chromosoma 123 (1-2), 3–13. https://doi.org/10.1007/s00412-013-0435-8.
Quénet, Delphine, McNally, James G., Dalal, Yamini, 2012. Through thick and thin The conundrum of chromatin fibre folding in vivo. EMBO Rep. 13 (11), 943–944. https://doi.org/10.1038/embor.2012.143.
Ricci, Maria Aurelia et al., 2015. Chromatin Fibers Are Formed by Heterogeneous Groups of Nucleosomes in Vivo. Cell 160 (6), 1145–1158. https://doi.org/10.1016/j.cell.2015.01.054. ISSN: 00928674. URL: https://linkinghub.elsevier.com/retrieve/pii/S0092867415001324 (visited on 07/25/2021).
Saberi, Abbas Ali, 2015. Recent advances in percolation theory and its applications. Phys. Rep., 1–32 https://doi.org/10.1016/j.physrep.2015.03.003. ISSN: 0370-1573.
Schreiber, Stuart L., Bernstein, Bradley E., 2002. Signaling Network Model of Chromatin. Cell 111 (6), 771–778. https://doi.org/10.1016/S0092-8674(02)01196-0. ISSN: 00928674. URL: https://linkinghub.elsevier.com/retrieve/pii/S0092867402011960 (visited on 07/24/2021).
Schwämmle, Veit, Jensen, Ole Nørregaard, 2013. A Computational Model for Histone Mark Propagation Reproduces the Distribution of Heterochromatin in Different Human Cell Types. PLoS ONE 8 (9). https://doi.org/10.1371/journal.pone.0073818. eprint: 1309.7157.
Sneppen, Kim, Micheelsen, Mille A., Dodd, Ian B., 2008. Ultrasensitive gene regulation by positive feedback loops in nucleosome modification. Mol. Syst. Biol. 4 (182), 1–5. https://doi.org/10.1038/msb.2008.21.
Szerlong, Heather J. et al., 2010. Activator-dependent p300 acetylation of chromatin in vitro: Enhancement of transcription by disruption of repressive nucleosome-nucleosome interactions. J. Biol. Chem. 285 (42), 31954–31964. https://doi.org/10.1074/jbc.M110.148718. ISSN: 00219258.
Tamaru, Hisashi, 2010. Confining euchromatin/heterochromatin territory: Jumonji crosses the line. Genes Develop. 24 (14), 1465–1478. https://doi.org/10.1101/gad.1941010.
Vignali, Marissa et al., 2000. Distribution of acetylated histones resulting from Gal4-VP16 recruitment of SAGA and NuA4 complexes. EMBO J. 19 (11), 2629–2640. https://doi.org/10.1093/emboj/19.11.2629.
Wang, Jiyong et al., 2014. Chromosome boundary elements and regulation of heterochromatin spreading. Cell. Mol. Life Sci. 71 (24), 4841–4852. https://doi.org/10.1007/s00018-014-1725-x.
Wang, Yaqi et al., 2020. Characterization of the chromatin accessibility in an Alzheimer's disease (AD) mouse model. Alzheimer's Res. Ther. 12 (1), 29. https://doi.org/10.1186/s13195-020-00598-2. ISSN: 1758-9193.
Wang, Liming, Nie, Qing, Enciso, German, 2010. Nonessential sites improve phosphorylation switch. Biophys. J. 99 (6), L41–L43. https://doi.org/10.1016/j.bpj.2010.07.030.
Wang, Jianrong, Lunyak, Victoria V., King Jordan, I., 2012. Genome-wide prediction and analysis of human chromatin boundary elements. Nucl. Acids Res. 40 (2), 511–529. https://doi.org/10.1093/nar/gkr750.
Wei, Gong Hong, Liu, De Pei, Liang, Chih Chuan, 2005. Chromatin domain boundaries: Insulators and beyond. Cell Res. 15 (4), 292–300. https://doi.org/10.1038/sj. cr.7290298.
Wu, Chenyi, Bassett, Andrew, Travers, Andrew, 2007. A variable topology for the 30-nm chromatin fibre. EMBO Rep. 8 (12), 1129–1134. https://doi.org/10.1038/sj.embor.7401115. ISSN: 1469-221X,1469-3178.
Zhou, Bing Rui et al., 2018. Revisit of Reconstituted 30-nm Nucleosome Arrays Reveals an Ensemble of Dynamic Structures. J. Mol. Biol. 430 (18), 3093–3110. https://doi.org/10.1016/j.jmb.2018.06.020.